

Beyond Nuclear Pasta: Phase Transitions and Neutrino Opacity of Non-Traditional Pasta

P. N. Alcain, P. A. Giménez Molinelli and C. O. Dorso
Departamento de Física, FCEyN, UBA and IFIBA, Conicet,
Pabellón 1, Ciudad Universitaria, 1428 Buenos Aires, Argentina and
IFIBA-CONICET
 (Dated: June 9, 2014)

In this work, we focus on different length scales within the dynamics of nucleons in conditions according to the neutron star crust, with a semiclassical molecular dynamics model, studying isospin symmetric matter at subsaturation densities. While varying the temperature, we find that a solid-liquid phase transition exists, that can be also characterized with a morphology transition. For higher temperatures, above this phase transition, we study the neutrino opacity, and find that in the liquid phase, the scattering of low momenta neutrinos remain high, even though the morphology of the structures differ significantly from those of the traditional nuclear pasta.

PACS numbers: PACS 24.10.Lx, 02.70.Ns, 26.60.Gj, 21.30.Fe

I. INTRODUCTION

A neutron star has a radius of approximately 10 km and a mass of a few solar masses. According to current models [1], the structure neutron star can be roughly described as composed in two parts: the *crust*, of 1.5 km thick and a density of up to half the normal nuclear density ρ_0 , with the structures known as *nuclear pasta* [2]; and the *core*, where the structure is still unknown and remains highly speculative [3]. Most neutron stars are remnants of core collapse supernovae. This kind of supernovae happen when the hot and dense Fe core of a dying massive star (known as proto-neutron star) collapses. During the collapse, several nuclear processes take place in the inner core of the star — electron capture, photodisintegration, URCA, etc. These processes, apart from increasing the overall neutron number of the system, produce a large amount of neutrinos which flow outwards. The interaction between the neutrinos streaming from the core of the proto-neutron star and its outer layers play an important role in reversing the collapse that causes the supernova.

On the other hand, neutron stars are born hot, but cool down by means of neutrino emission. Therefore, the interaction between the neutrinos and neutron star matter is key to comprehend two aspects of a neutron star history: its genesis and its thermal evolution.

The neutron stars' crust is composed of neutrons and protons embedded in a degenerate electron gas. Protons and neutrons in the crust are supposedly arranged in structures that differ substantially from the “normal” nuclei — the non-homogeneous phases collectively known as *nuclear pasta*. The structure of this nuclear pasta is related to the neutrino opacity of neutron stars' crust, neutron star quakes, and pulsar glitches. Specifically, the neutron star quakes and pulsar glitches are related to the mechanical properties of the crust matter [4], while the neutrino opacity is enhanced by coherent scattering. This enhancement of the crust's opacity is related to the

static structure factor of nuclear pasta [5]:

$$\frac{d\sigma}{d\Omega} = \left(\frac{d\sigma}{d\Omega} \right)_{\text{uniform}} \times S(q).$$

And since neutron stars cooling is associated with neutrino emission from the core, the interaction between the neutrinos and the particular structure of the crust would dramatically affect the thermal history of young neutron stars.

Several models have been developed to study nuclear pasta, and they have shown that these structures arise due to the interplay between nuclear and Coulomb forces in an infinite medium. Nevertheless, the dependence of the thermodynamic observables has not been studied in depth.

The original works of Ravenhall *et al.* [2] and Hashimoto *et al.* [6] used a compressible liquid drop model, and proposed the now known as *pasta phases* — *lasagna*, *spaghetti* and *gnocchi*—. Further works [7–12] analyzed only these phases, with mean field models. Other authors [13–16] used dynamical models, but focusing mainly on the phases already mentioned. The work by Nakazato *et al.* [18], inspired by polymer systems, found also gyroid and double-diamond structures, with a compressible liquid drop model. Dorso *et al.* [17] arrived to pasta phases different from those already mentioned with molecular dynamics, studying mostly its characterization at very low temperatures.

In this work, we study the neutron stars with molecular dynamics, using the CMD model [22]. We use morphologic and thermodynamic tools to characterize symmetric neutron star matter at different temperatures, focusing on the static structure factor. We characterize the morphology of the emerging structures with the pair distribution function and the *Minkowski functionals* [15], a complete set of morphological measures. The possible existence of a solid-liquid phase transition is explored via the Lindemann coefficient [19].

With these tools at very low temperatures, we found a phase transition that is both morphologic and thermo-

dynamic: a discontinuity in the Minkowski functionals shows the morphologic transition, while a coincident discontinuity in both energy and the Lindemann coefficient show a thermodynamic solid-liquid transition. At temperatures slightly higher, we found stable structures that do not belong to usual pasta menu. Moreover, these unusual shapes absorb neutrinos more efficiently than the typical nuclear pasta.

This work is structured as follows. In section II we review the interaction model, along with the tools used to analyze the results we obtained. In section III A we present and characterize the solid-liquid phase transition in nuclear pasta. Then, in sections III B and III C we study the very-long range order of the pasta phases, focusing on its influence on the opacity of the crust to low-momentum neutrinos. We discuss the appearance of some unusual pasta shapes, and how these newfound structures may enhance the opacity of the crust more than traditional *pasta* in section III D. Finally, in section IV we draw conclusions about the results presented.

II. CLASSICAL MOLECULAR DYNAMICS MODEL

Of the many models used to study nuclear pasta, the advantage of classical or semiclassical models is the accessibility to position and momentum of all particles at all times. This allows the study of the structure of the nuclear medium from a particle-wise point of view. Many models exist with this goal, like simple-semiclassical potential [16], quantum molecular dynamics [21] and classical molecular dynamics [22]. In these models the Pauli repulsion between nucleons of equal isospin is either hard-coded in the interaction or as a separate term [23].

In this work, we model the interaction between nucleons with a classical molecular dynamics (CMD) model to study nuclear reactions. Dorso *et al.* provided justification for its use in the stellar crust environment [17].

The classical molecular dynamics model CMD, as introduced in Ref. [24], has been successfully used in heavy-ion reaction studies to: help understand experimental data [25]; identify phase-transition signals and other critical phenomena [26–29]; and explore the caloric curve [30] and isoscaling [31, 32]. CMD uses two two-body potentials to describe the interaction of nucleons, which are a combination of Yukawa potentials:

$$V_{np}(r) = v_r \exp(-\mu_r r)/r - v_a \exp(-\mu_a r)/r$$

$$V_{nn}(r) = v_0 \exp(-\mu_0 r)/r$$

where V_{np} is the potential between a neutron and a proton, and V_{nn} is the repulsive interaction between either nn or pp . The cutoff radius is $r_c = 5.4$ fm and for $r > r_c$ both potentials are set to zero. The Yukawa parameters μ_r , μ_a and μ_0 were determined to yield an equilibrium density of $\rho_0 = 0.16$ fm⁻³, a binding energy $E(\rho_0) = 16$ MeV/nucleon and a compressibility of 250 MeV [22].

To simulate an infinite medium, we used CMD under periodic boundary conditions, symmetric in isospin (i.e. with $x = Z/A = 0.5$, 2500 protons and 2500 neutrons) in cubical boxes with sizes adjusted to have densities between $\rho = 0.03$ fm⁻³ $\leq \rho \leq 0.13$ fm⁻³. Although in the actual neutron stars the proton fraction is low ($x < 0.5$), we chose to work with symmetric matter because that way we could study the neutron stars without having a symmetry term in the energy.

A. Coulomb interaction in the Model

Since a neutralizing electron gas embeds the nucleons in the neutron star crust, the Coulomb forces between protons are screened. One of the many ways to model this screening effect is the Thomas–Fermi approximation, used with various nuclear models [5, 13, 17]. According to this approximation, protons interact via a Yukawa-like potential, with a screening length λ :

$$V_{TF}(r) = q^2 \frac{e^{-r/\lambda}}{r}.$$

Theoretical estimations for the screening length λ are $\lambda \sim 100$ fm [33], but we set the screening length to $\lambda = 20$ fm. This choice was based on previous studies [34], where we have shown that this value is enough to adequately reproduce the expected length scale of density fluctuations for this model.

B. Simulation procedure

The trajectories of the nucleons are then governed by the Pandharipande and the screened Coulomb potentials. The nuclear system is cooled from $T = 0.8$ MeV to $T = 0.2$ MeV using isothermal molecular dynamics with the Nosé–Hoover thermostat procedure [35], in the LAMMPS package [36]. Systems are cooled in small temperature steps ($\Delta T = 0.01$), decreasing the temperature once both the energy and the temperature, as well as their fluctuations, are stable.

C. Other tools

1. Minkowski functionals

The Minkowski functionals [37] are a set of independent functionals that satisfy three properties: motion invariance, additivity and continuity. The morphological and topological properties of any given closed and oriented surface can be completely characterized by these Minkowski functionals [34, 38]. According to Hadwiger’s theorem [39], for a body in a d -dimensional Euclidean space, there are $d + 1$ Minkowski functionals. For three dimensional bodies, these four functionals are: volume V ,

surface area S , Euler characteristic χ and integral mean curvature B .

While the volume and surface area have an easy intuitive interpretation, we will explain further the other two functionals. The Euler characteristic χ is a topological measure that can be interpreted as:

$$\chi = (\text{isolated regions}) + (\text{cavities}) - (\text{tunnels})$$

. The integral mean curvature, known as *mean breadth*, is a measure of the typical width of the body.

Using these functionals, we proposed a classification for the structures obtained in simulations of Neutron Star Matter within the CMD framework that is summarized in table I [17].

TABLE I: Classification of NSM shapes based on Minkowski functionals

	$B < 0$	$B \sim 0$	$B > 0$
$\chi > 0$	Anti-Gnocchi		Gnocchi
$\chi \sim 0$	Anti-Spaghetti	Lasagna	Spaghetti
$\chi < 0$	Anti-Jungle Gym		Jungle Gym

2. Lindemann coefficient

The Lindemann coefficient [19] is based on the idea of particle “disorder”, used mostly to study solid-liquid transitions in infinite systems like crystals [40] and is defined from the standard deviation of the positions of the particles Δr_i^2 as follows :

$$\Delta_L = \frac{\sqrt{\sum_i \langle \Delta r_i^2 / N \rangle}}{a}$$

where a is the lattice constant of the crystal and N is the total number of particles. In our case, we set $a = (V/N)^{1/3}$, the typical length of each particle.

III. RESULTS AND DISCUSSION

In what follows, we present the results obtained cooling down a system of approximately 5000 particles.

A. Phase transition

1. Thermodynamical Phase Transition

Figure 1 presents the energy as a function of temperature (caloric curve), for several densities. Each of these densities exhibit a discontinuity in the energy at certain temperatures — a signal of a first order phase transition.

This transition can be confirmed and further characterized as a solid-liquid phase transition by looking at the Lindemann coefficient. The Lindemann coefficient for $\rho = 0.05 \text{ fm}^{-3}$ as a function of temperature, can be seen in figure 2, along the energy. This figure shows that the discontinuities in Lindemann coefficient and in energy are at the same temperature. These two factors are, effectively, the signature of a solid-liquid phase transition.

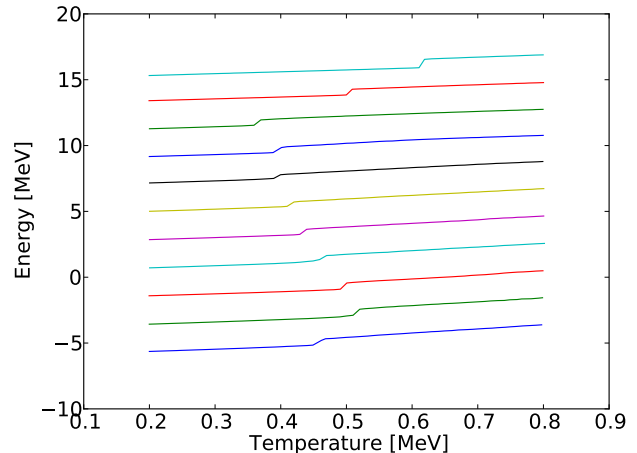


FIG. 1: Energy as a function of temperature for different densities. We see that there is a discontinuity in the range of $T_l = 0.35 \text{ MeV}$ to $T_h = 0.65 \text{ MeV}$, depending on the density, a signal of a first-order phase transition. In the figure, densities range from $\rho = 0.03 \text{ fm}^{-3}$ and $\rho = 0.13 \text{ fm}^{-3}$, increasing $\Delta\rho = 0.01 \text{ fm}^{-3}$ upwards.

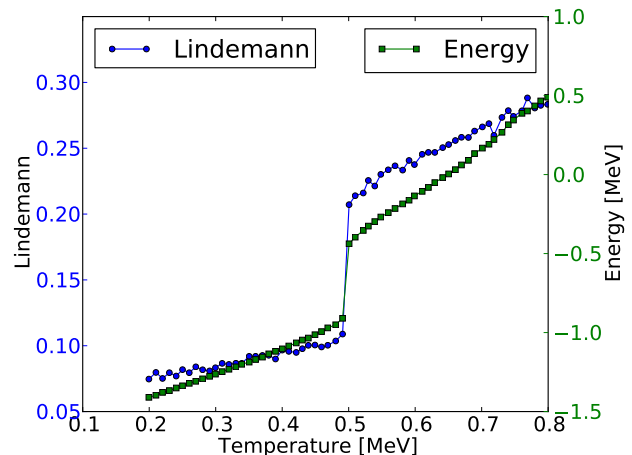


FIG. 2: Lindemann coefficient and energy as a function of temperature for a chosen density, $\rho = 0.05 \text{ fm}^{-3}$. The sudden change in their value is a signal of a solid-liquid phase transition. We can see that both discontinuities are at the same temperature

In figure 3 we show the radial distribution function for three different densities: $\rho = 0.03 \text{ fm}^{-3}$ (*spaghetti*), $\rho = 0.05 \text{ fm}^{-3}$ (*lasagna*) and $\rho = 0.08 \text{ fm}^{-3}$ (tunnels), just above and below the transition temperature, as well as a snapshot of the system at the high temperature phase. Since the first peaks (corresponding to the nearest neighbors) are at the same position regardless of the temperature, we conclude that the short range order is present both above and below the transition. However, the peaks for third and higher order neighbors, distinctive of solid phases, disappear as the temperature is increased through the transition. The very-long range order also survives the transition, as discussed further in section III B

2. Morphological Phase Transition

When we look at the Minkowski functionals, particularly the Euler characteristic and the mean breadth, we can see that there is again a “critical” temperature at which both the Euler characteristic and the mean breadth show a sharp transition. We show, as an example, these magnitudes as a function of temperature for density $\rho = 0.05 \text{ fm}^{-3}$ in figure 4. As this transition is signaled by morphological observables, we conclude that this transition is morphological.

These signals of a solid-liquid phase transition (energy and Lindemann’s coefficient discontinuity) and morphological transition (Minkowski functionals discontinuity) point at the same transition temperature, as can be seen in the phase diagram of figure 5. This means that as the systems are cooled down at fixed volume, they undergo a thermodynamical and a morphological phase transition, and they do so at the same temperature.

B. Very Long-range Behavior

On top of the disappearance of the long range order characteristic of solids, another feature becomes evident from figure 3. As temperature increases through the solid-liquid transition, a very-long range modulation in the pair correlation function survives. This very long range ordering is characteristic of the pasta phases. In figure 6, a visual representation of the spatial configuration for $\rho = 0.05 \text{ fm}^{-3}$ is shown, for temperatures both below and above the transition. In it, we show that not only the solid phase has the usual pasta shape, but the liquid phase preserves it. Below the transition, we have “frozen pasta”. Just above it, nucleons may flow but confined to a certain pasta or pasta-like structure, as we shall see in the following sections.

C. Neutrino transport properties

This very long-range order, evident from figure 3, is responsible for a peak at very low momentum k ($\sim 10 \text{ fm}^{-1}$ wave-length) in the static structure factor $S(k)$, proportional to the particle scattering probability. With this in mind, we now put the focus on the very long-range order of our structures.

In figure 7 we plot the height of the low momenta peak $S(k < 0.5 \text{ fm}^{-1})$ ($\lambda \gtrsim 13 \text{ fm}$) as a function of the temperature for $\rho = 0.05 \text{ fm}^{-3}$. The most clear and intuitive way to read this figure is backwards, from high to low temperatures, tracing the cooling procedure each system undergoes in our simulations. Each line in the figure corresponds to evolutions with different initial conditions but following the same protocol for cooling down and the same criteria for stability.

At high temperatures the nucleons are rather uniformly distributed and no structure is evidenced by $S(k)$: the “peak” vanishes as its height tends to 1, the value for homogeneous systems. As the temperature is decreased, a peak at low momentum develops. The transition described in sections III A and III A 2, manifests in figure 7 as the vanishing of fluctuations below the transition temperature $T \lesssim 0.5 \text{ MeV}$. Even at temperatures as high as $T = 1.0 \text{ MeV}$ there is still a recognizable low momentum absorption peak (with height well over 1), but it does not always correspond to a usual pasta (*gnocchi*, *spaghetti* or *lasagna*) in our simulations. At such high temperatures and for most densities, the system is in a “sponge-like” structure which is, nevertheless, ordered enough to produce a recognizable peak in $S(k)$.

Interestingly, when the cooling procedure drives the system at temperatures below $T \sim 0.7 \text{ MeV}$, we observe that in different runs the system may collapse into several distinct structures, in addition to the usual lasagna which is the ground state at this density. A zoom into the $S(k)$ peak’s height for this region of temperatures can be found in figure 8, and snapshots of the structures corresponding to each of those runs can be seen in figure 9 (see captions for details).

D. Properties of non-traditional pasta

Usual pasta shapes are ground states (potential energy minima). The nontraditional structures described in the previous section are likely to be local potential energy minima, which abound in frustrated systems like this. The complexity of the energy landscape (many local minima separated by energy barriers) makes it difficult to reach the actual ground state by simple cooling in molecular dynamics simulations. However, since we are working at fixed number of particles, volume and temperature ((N, V, T) ensemble), the equilibrium state of the system at finite temperatures is not that which minimizes the internal energy but that which minimizes the Helmholtz free energy, $A = E - TS$. All of these struc-

tures may then be actual equilibrium solutions, as long as they are free energy minima.

Accurate calculation of free energies from MD simulations is computationally very expensive [20, pp. 167-200], specially at low temperatures when overcoming energy barriers become very improbable events. However, we can easily compute the internal energy distributions over a long evolution at constant temperature. In figure 10 we show internal energy histograms constructed from very long thermalized evolutions at $T = 0.6$ MeV using three of the systems shown in 9 as initial conditions. We see that, although the histograms clearly differ, they overlap significantly. This fact indicates that the full ensemble of equilibrium configurations at $T = 0.6$ MeV contains all of these structures, not only lasagna. In light of this we propose that at low but finite temperatures, the state of the system should be described as an ensemble of both traditional and nontraditional structures rather than by a single one.

When we heat up the system to $T = 0.8$ MeV, these three histograms become indistinguishable, hinting that, for this temperature, the free energy barriers can be overcome, and the system is more likely to be ergodic.

These observations are relevant because all of these structures show peaks in $S(k)$ at the same wavelenght (within the uncertainty), although of different heights. And more importantly, we find from our calculations that the seemingly amorphous, sponge-like structures can be more efficient in scattering neutrinos of the same momentum than any usual pasta (i.e. have higher peaks), usually invoked as a necessity for coherent neutrino scattering. This result shows that unusual pasta shapes should also be considered when studying the structure of a neutron star's crust.

IV. DISCUSSION AND CONCLUDING REMARKS

In this work we used a classical molecular dynamics model to study symmetric neutron star matter for different temperatures. We found a solid-liquid phase transition takes place for every density at very low temperatures. This transition was characterized with the Lin-

demann coefficient and by a discontinuity in the caloric curves. The transition is also signaled by a discontinuity in the Minkowski functionals as a function of the temperature, and all three indicators gave the same transitions temperature. This phase transition doesn't alter the typical pasta shape (*lasagna* and *spaghetti* in the cases shown): the liquid phase preserves the pasta shape found in the solid phase (the ground state).

As we increase the temperature beyond $T = 0.7$ MeV, the typical pasta shapes become unstable and the system adopts slightly less ordered but still inhomogeneous structures. However, the low momentum absorption peak of this structures remains quite high. This implies that the existence of traditional pasta shapes –which are only obtained at extremely low temperatures– is not a necessary condition for the enhancement of the neutrino absorption in a neutron star's crust.

Furthermore, we also found that at $T \sim 0.7$ MeV the system can exist in various stable states, all of them with different morphology –and, consequently, different structure factor–, but very close in internal energy. From our simulations at fixed (N, V, T) , these states appear to be separated by relatively high energy barriers which make the spontaneous transition between them a very improbable event, and unlikely to be observed within a single simulation run. However, the energy distributions obtained from long enough runs starting from different states overlap significantly, indicating that all of them are members of the full ensemble of equilibrium states at that temperature. At $T \sim 0.8$ MeV the energy barriers become surmountable and the energy histograms completely overlap.

All of this suggests that the actual state of these systems at low, but finite temperatures, is better described as an ensemble of shapes rather than by a single pasta-like structure.

ACKNOWLEDGMENTS

C.O.D. is a member of the Carrera de Investigador CONICET, work partially supported by CONICET Grant PIP0871. P.G.M. and P.N.A. by a CONICET grant. The three-dimensional figures were prepared using Visual Molecular Dynamics [41].

-
- [1] D. Page, J. M. Lattimer, M. Prakash and A. W. Steiner, *Astrophys. J. Supp.* **155**, 623 (2004)
 - [2] D. G. Ravenhall, C. J. Pethick and J. R. Wilson, *Phys. Rev. Lett.* **50**, 2066 (1983).
 - [3] S. Woosley and T. Janka, *Nature Phys.* **1**, 147 (2005)
 - [4] Y. Mochizuki and T. Izuyama, *Astrophys. J.* **440**, 263 (1995).
 - [5] C.J. Horowitz, M.A. Perez-Garcia, and J. Piekarewicz, *Phys. Rev.* **C69**, 045804 (2004).
 - [6] M. Hashimoto, H. Seki and M. Yamada, *Prog. Theor.*

- Phys.* **71**, 320 (1984).
- [7] R. D. Williams and S. E. Koonin, *Nucl. Phys.* **A435**, 844 (1985).
- [8] K. Oyamatsu, *Nucl. Phys.* **A561**, 431 (1993).
- [9] C. P. Lorenz, D. G. Ravenhall and C. J. Pethick, *Phys.Rev. Lett.* **70**, 379 (1993).
- [10] K. S. Cheng, C. C. Yao and Z. G. Dai, *Phys. Rev.* **C55**, 2092 (1997).
- [11] G. Watanabe, K. Iida and K. Sato, *Nucl. Phys.* **A676**, 445 (2000).

- [12] G. Watanabe and K. Iida, Phys. Rev. **C68**, 045801 (2003).
- [13] T. Maruyama, K. Niita, K. Oyamatsu, T. Maruyama, S. Chiba and A. Iwamoto, Phys. Rev. **C57**, 655 (1998).
- [14] T. Kido, Toshiki Maruyama, K. Niita and S. Chiba, Nucl. Phys. **A663-664**, 877 (2000).
- [15] G. Watanabe, K. Sato, K. Yasuoka and T. Ebisuzaki, Phys. Rev. **C66**, 012801 (2002).
- [16] C. J. Horowitz, M. A. Pérez-Garcia, J. Carriere, D. K. Berry, and J. Piekarewicz, Phys. Rev. **C70**, 065806 (2004).
- [17] C.O. Dorso, P.A. Giménez Molinelli and J.A. López, Phys. Rev. **C86**, 055805 (2012).
- [18] K.I. Nakazato, K. Oyamatsu and S. Yamada, Phys. Rev. Lett. **103** 132501 (2009)
- [19] F.A. Lindemann, Physik. Z. **11**, 609 (1910).
- [20] D. Frenkel and B. Smit, "Understanding Molecular Simulations", 2nd Ed., Academic Press (2002).
- [21] T. Maruyama, K. Niita, K. Oyamatsu, T. Maruyama, S. Chiba, A. Iwamoto, Phys. Rev. **C57**, 655 (1998)
- [22] A. Vicentini, G. Jacucci and V. R. Pandharipande, Phys. Rev. **C31**, 1783 (1985); R. J. Lenk and V. R. Pandharipande, Phys. Rev. **C34**, 177 (1986); R.J. Lenk, T.J. Schlagel and V. R. Pandharipande, Phys. Rev. **C42**, 372 (1990).
- [23] C.O. Dorso and J. Randrup, Phys. Lett. **B215**, 611 (1988)
- [24] A. Barrañón, C.O. Dorso, J.A. López and J. Morales, Rev. Mex. Fís. **45**, 110 (1999).
- [25] A. Chernomoretz, L. Gingras, Y. Larochelle, L. Beaulieu, R. Roy, C. St-Pierre and C. O. Dorso, Phys. Rev. **C65**, 054613 (2002).
- [26] A. Barrañón, C.O. Dorso and J.A. López, Rev. Mex. Fís. **47-Sup. 2**, 93 (2001).
- [27] A. Barrañón, C.O. Dorso, and J.A. López, Nuclear Phys. **A791**, 222 (2007).
- [28] A. Barrañón, R. Cárdenas, C.O. Dorso, and J.A. López, Heavy Ion Phys. **17**, 59 (2003).
- [29] C.O. Dorso and J.A. López, Phys. Rev. **C64**, 027602 (2001).
- [30] A. Barrañón, J. Escamilla Roa and J.A. López, Phys. Rev. **C69**, 014601 (2004).
- [31] C.O. Dorso, C.R. Escudero, M. Ison and J.A. López, Phys. Rev. **C73**, 044601 (2006).
- [32] C.O. Dorso, P.A. Giménez Molinelli and J.A. López, J. Phys. G: Nucl. Part. Phys. **38**, 115101 (2011); *ibid*, Rev. Mex. Phys., **S 57 (1)**, 14 (2011).
- [33] A. L. Fetter and J. D. Wallecka, *Quantum Theory of Many-Particle Systems*, McGraw-Hill (1971)
- [34] P. N. Alcain, P. A. Giménez Molinelli, J. I. Nichols, C. O. Dorso, Phys. Rev. **C89**, 055801 (2014)
- [35] S. Nose, J. Chem. Phys. **81**, 511 (1984)
- [36] S. Plimpton, J. Comp. Phys., **117**, 1-19 (1995)
- [37] K. Michielsen and H. De Raedt, Phys. Reports **347**, 461 (2001).
- [38] G. Watanabe, K. Sato, K. Yasuoka and T. Ebisuzaki, Phys. Rev. **C68**, 035806 (2003)
- [39] Klain, D.A.; Rota, G.-C. (1997). Introduction to geometric probability. Cambridge: Cambridge University Press.
- [40] J. H. Bilgram, Phys. Rep. **153**, 1 (1987)
- [41] Humphrey, W., Dalke, A. and Schulten, K., 'VMD - Visual Molecular Dynamics', J. Molec. Graphics **14.1**, 33 (1996).

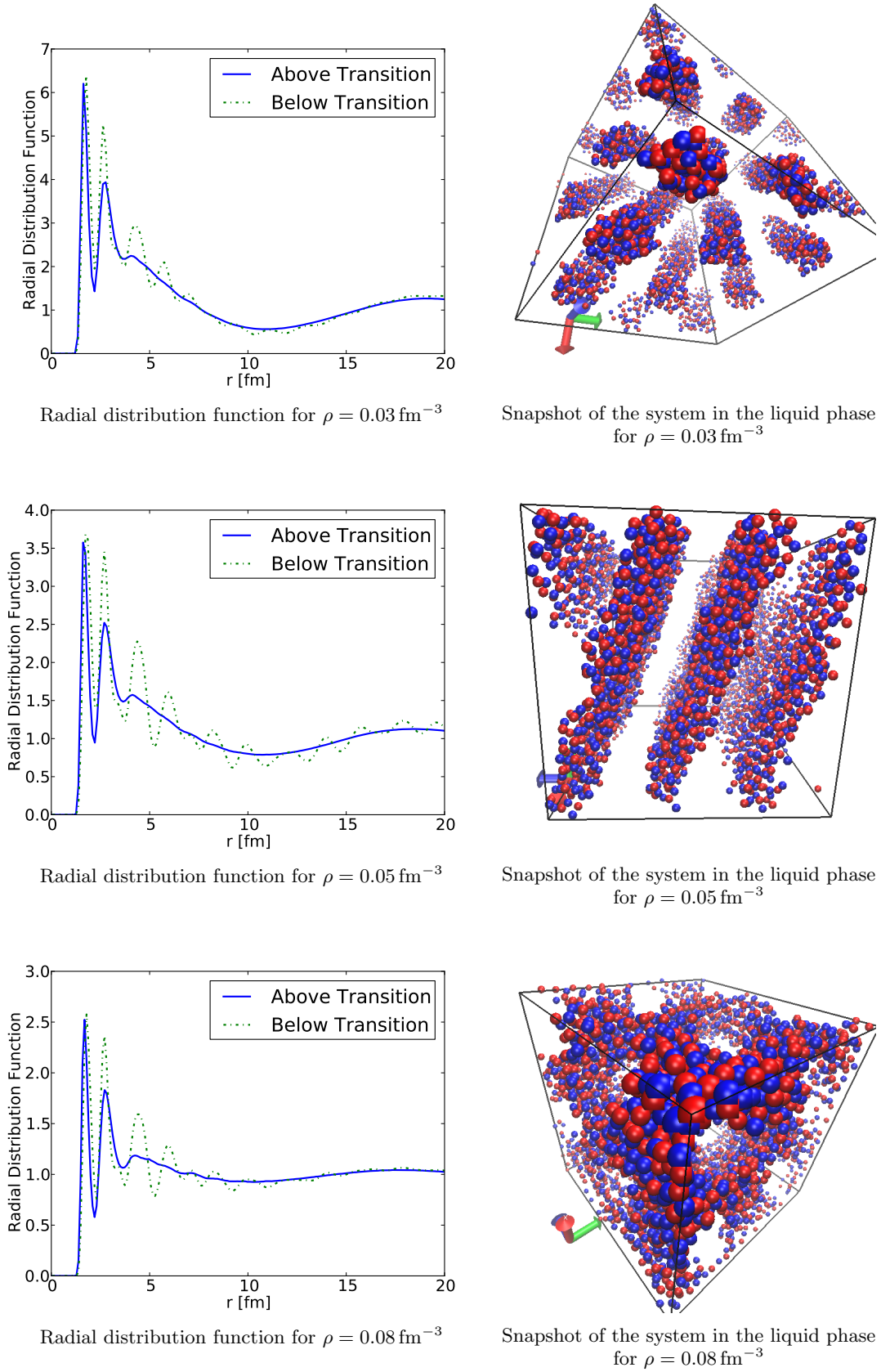


FIG. 3: Radial distribution function for different densities, both below and above the transition temperature, and snapshots of the system in the liquid phase. Although the first peaks of the distribution are in the same position for both temperatures, the following peaks, which exhibit a long-range order typical of solids, are only present below the transition temperature.

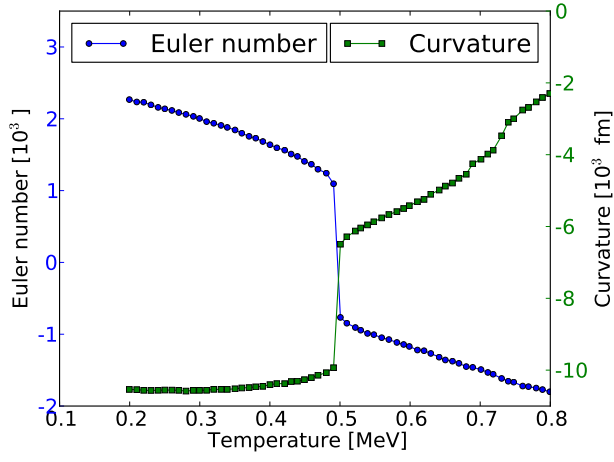


FIG. 4: Euler number and mean breadth for $\rho = 0.05 \text{ fm}^{-3}$. We observe a sharp transition for both Minkowski functionals.

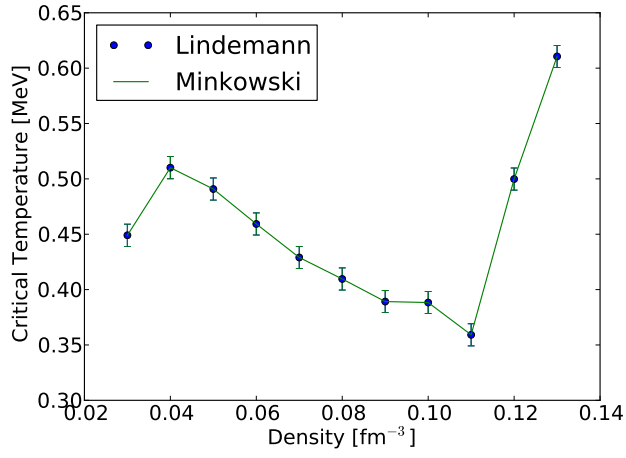


FIG. 5: Critical temperature as a function of density. We see the overlap between the Minkowski and the Lindeman critical temperature.

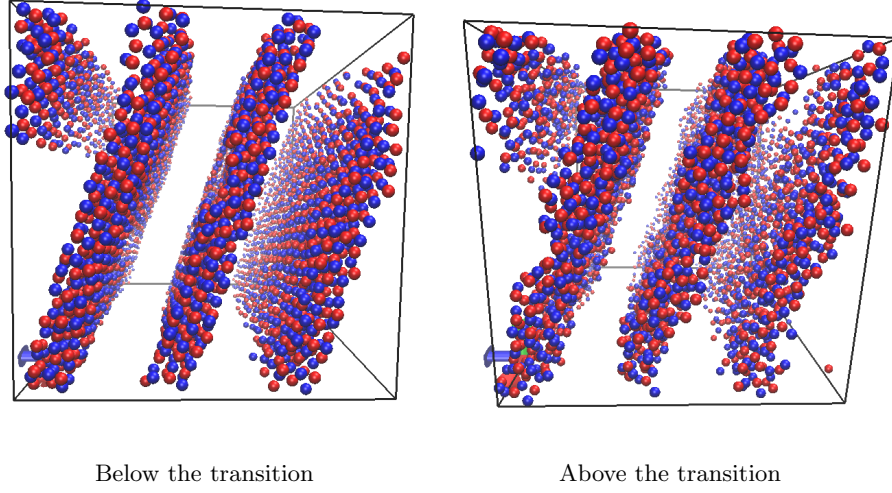


FIG. 6: Spatial distribution for $\rho = 0.05 \text{ fm}^{-3}$, both above and below the transition temperature. The structures are similar, but much more disordered above the transition.

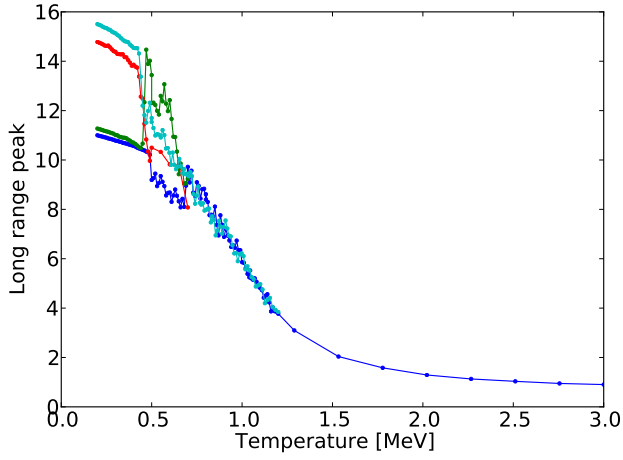


FIG. 7: Peak of $S(k)$ for low momenta as a function of the temperature, for $\rho = 0.05 \text{ fm}^{-3}$. We see two behaviors, for $T < 0.5 \text{ MeV}$ and $T > 0.5 \text{ MeV}$.

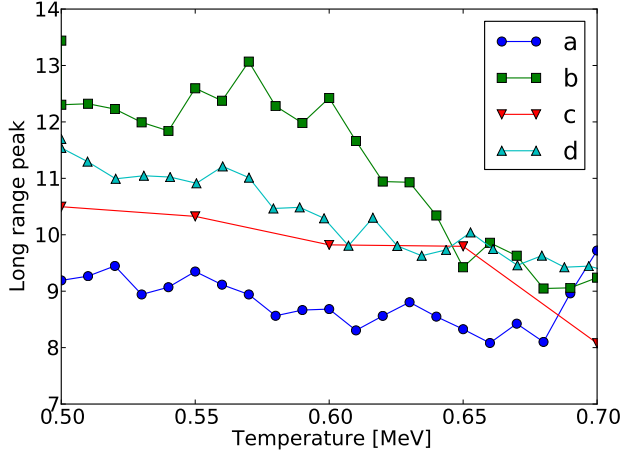


FIG. 8: Peak of $S(k)$ for low momenta: zoom into the temperature region between $T = 0.5$ MeV and $T = 0.7$ MeV. We can see that distinct runs yield different absorption peaks for low momenta.

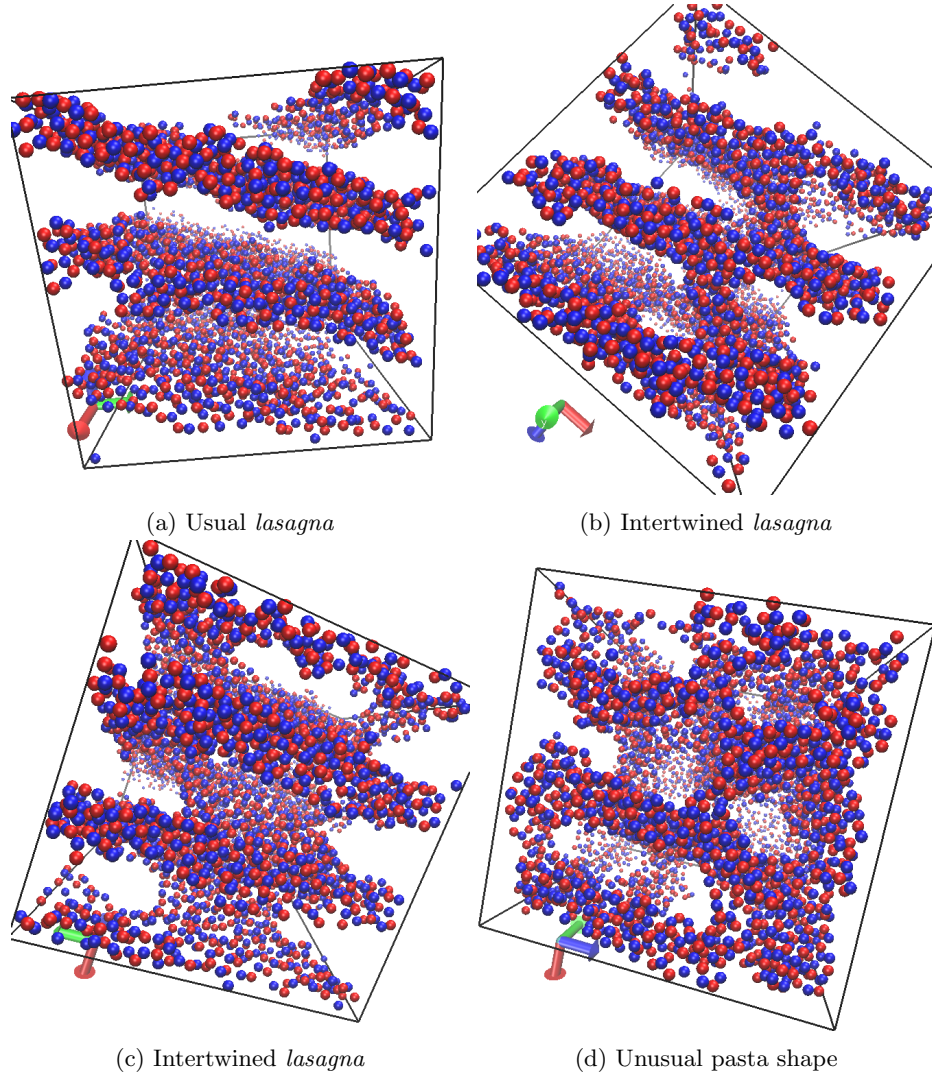
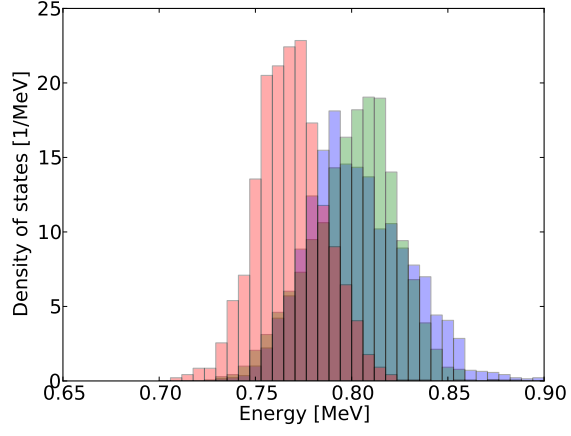
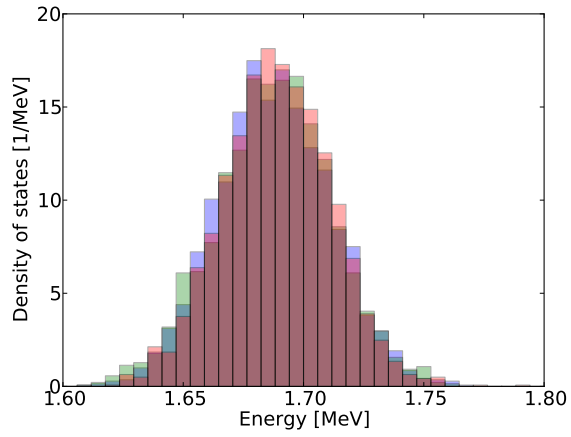


FIG. 9: Spatial distribution for $\rho = 0.05 \text{ fm}^{-3}$ for different initial conditions. We see that we have the usual *lasagna*, but also intertwined *lasagnas* and other structures that don't resemble usual pasta. Despite being different from the usual pasta phases, these shapes have a peak for low momentum in the structure factor.



(a) Distribution of energies for $T = 0.6$ MeV



(b) Distribution of energies for $T = 0.8$ MeV

FIG. 10: Energy distribution for a canonical ensemble.

It can be seen that, for $T = 0.8$ MeV, all three distributions overlap completely. However, in $T = 0.6$ MeV, the histograms, albeit split, still overlap significantly.